M*D21 (MYD21/MOD21) and M*D11 (MYD11/MYD21) Land Surface Temperature and Emissivity (LST&E) Products Status Report

Glynn Hulley,
NASA Jet Propulsion Laboratory, California Institute of Technology

Jaime Nickeson,
NASA Goddard Space Flight Center

5 August 2020

1 Background

Currently two different LST&E product streams exist for distribution at the NASA LPDAAC—the original M*D11 products and the newer M*D21 suite of products released in 2018 (Table 1). The M*D11 products are produced from the generalized split-window (GSW) [1] and day/night pair [2] algorithms, while the M*D21 products are created using the temperature emissivity separation (TES) algorithm [3-5]. The primary algorithm for producing the M*D11 1 km product is the GSW algorithm (M*D11A1/A2) [1]. In this algorithm, emissivities are assigned according to a land classification scheme [6], and the atmospheric effects are compensated for by using the differential absorption features from two longwave window bands (bands 31, 32). This GSW approach has been used with much success over oceans to compute sea surface temperature, and works well over densely vegetated areas and inland water bodies where the assumption of a single fixed emissivity is valid [7]. However, several studies have documented a cold bias of 3-5 K with the GSW approach over dryland regions (arid and semi-arid). This primarily arises because these regions have much higher variability in emissivity both spectrally and spatially, yet only a single emissivity value is assigned ('barren' land class) that usually overestimates the emissivity [3, 8, 9]. This is a significant drawback considering that dryland regions constitute about 33% of the Earth's land surface, and the resulting errors far exceed the specified product accuracy of 1 K [1]. Moreover, by fixing the emissivity and not allowing it to vary dynamically as the land cover type changes, the emissivity cannot be used to study land cover changes, such as those from desertification [10].

The second M*D11 algorithm (M*D11B1), uses a day/night approach, where the additional information from two scenes over the same location, with differing daytime and nighttime atmospheres and an assumed constant emissivity, are used to dynamically retrieve the LST and emissivity using 7 thermal bands [2]. Although LST&E are dynamically retrieved, the approach is limited by multiple factors, including the need to accurately co-register the day and

night scenes, cloud contamination, and saturation of the mid-wave infrared (MIR) bands over very warm targets. As a result, the M*D11B1 product is retrieved at ~5-6 km as opposed to the nominal 1 km generated by the MODIS sensor. This resolution limits the utility of M*11B1 in field-scale (<1 km^2) types of applications, and thus the M*D11B1 LST&E products have been largely used for mean monthly climate modeling applications [11]. One major advantage of the M*D11B1 product is that emissivities are also retrieved for the MIR bands of MODIS (bands 20, 22, 23), and these are used in other products like the NASA MEaSUREs Combined ASTER and MODIS Emissivity for Land (CAMEL) [12] product that produces hyperspectral emissivity in the MIR and TIR ranges from the M*D11C3 products and are used extensively in the satellite sounder retrieval community for retrieving water vapor and air temperature profiles [13, 14]

The issues outlined above for these two algorithms have largely been addressed by applying the Advanced Spaceborne Thermal Emission and Reflection Radiometer (ASTER) temperature emissivity separation (TES) algorithm to retrieve LST&E from MODIS (M*D21) data at 1 km resolution using the three TIR bands 29, 31 and 32 [3, 5] (see product differences in Table 1). The TES algorithm uses an emissivity model based on the variability in the surface radiance data to dynamically retrieve both LST and spectral emissivity (Gillespie et al. 1998). Initial validation and evaluation of the M*D21 products have shown similar accuracy to M*D11 over vegetated and ice/snow surfaces, while there is significant improvement in accuracy over dryland regions, with biases reduced from 3-5 K to even <1 K (see Table 2 and Figure 1). The M*D21 products also include a dynamically-retrieved multispectral emissivity (bands 29, 31, and 32), twice-daily, and at 1 km resolution. This has enabled the use of MODIS emissivity data to monitor land cover and land use changes associated with changes in soil moisture [15, 16], monitoring melt zones on glaciers [17, 18], as well as the assessment of land cover change and degradation [10, 18].

2 MODIS LST&E L2 swath product characteristics

Table 1. A summary of characteristics and differences between the MODIS M*D21 and M*D11 level-2 swath LST&E products (differences highlighted in bold).

	M*D11_L2	M*D21_L2
Dimensions	Swath (2030 x 1354)	Swath (2030 x 1354)
Spatial resolution	~1-km at nadir	~1-km at nadir
Temporal resolution	Twice-daily LST **Emissivity fixed day and night**	Twice-daily LST **Twice-daily Emissivity**
Algorithm	**Split-window**	**TES algorithm**
Output products	LST, **Classification Emissivity (bands 31, 32)**	LST, **Retrieved Emissivity (bands 29, 31, 32)**

3 Published Validation Results

Table 2. A summary of MODIS MYD21 and MYD11 LST validation results of studies where the validation was performed for both products simultaneously, i.e. 1-1 validation comparison with in situ data.

Reference(s)	Surface Type and Location	LST (RMSE)	
		MYD11	MYD21
Malakar and Hulley 2016 [3]	vegetation, water (4 sites, U.S.A)	1.0 K	1.2 K
	arid, semi-arid (6 sand dune sites, U.S.A)	3.3 K	1.1 K
Li et al. 2020 [8]	arid, semi-arid (10 sand dune sites, China)	3.0 K	1.9 K
Coll et al. 2016 [19]	vegetation (rice paddy, Spain)	0.6 K	0.6 K
Ermida et al. 2014 [20]	vegetation (oak woodland, Portugal)	2.4 K	1.5 K

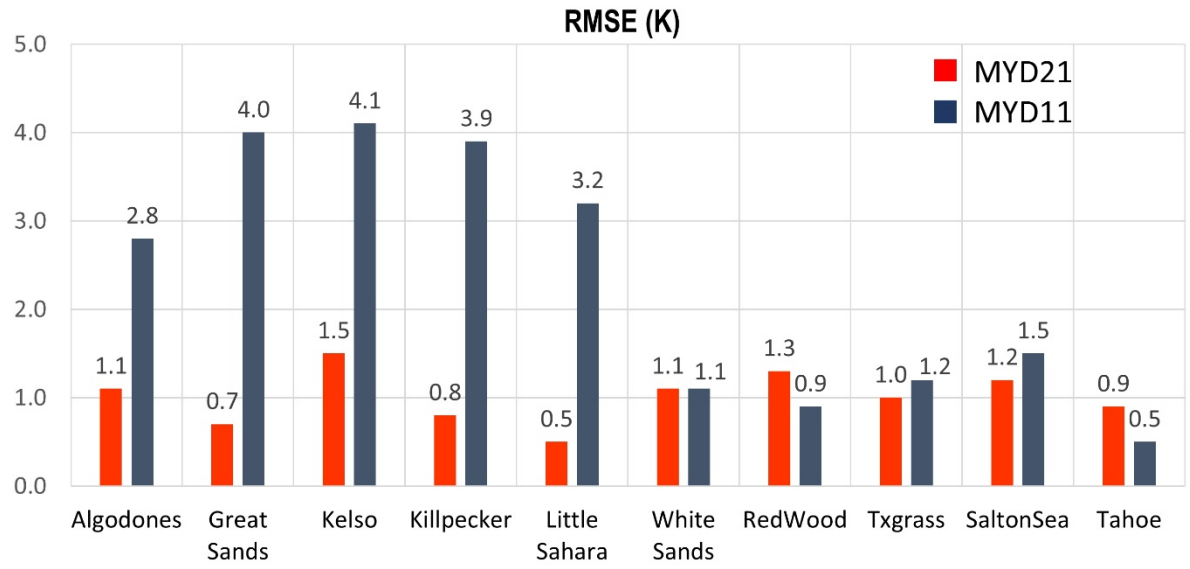

Figure 1. Summary of LST validation of the MYD21 and MYD11 C6 products from 2002-2018 using a combination of Temperature-based and Radiance-based validation methods at 2 water, 2 vegetated, and 6 pseudo-invariant sand dunes sites in the U.SA [3, 21].

4 Product Status

Notes (as of: 08/04/2020). See Table 3 for summary.

- The Terra MOD21 LSTE products in Collection 6 (C6) were affected by the band 29 crosstalk calibration issue and were only produced up to 2005 in C6 as a result. This issue has been addressed in C6.1 with updated calibration and all Terra products are currently being reprocessed. All Aqua MYD21 LSTE products are available in C6.
- New M*D21C1/C2/C3 climate modeling grid (CMG) products will be available in C6.1, similar to the M*D11C* products, except they will not yet include emissivities for the MIR bands 20, 22, and 23. This will be implemented in C7.
- In C6.1 the M*D21 products will have the capability of near-real time processing of the Level 2 swath and daily/8-day sinusoidal gridded products using daily GEOS-5 atmospheric data (as opposed to MERRA-2 data with one-month latency).

Table 3. Current MODIS LST&E products (M*D21*, M*D11*) in Collection 6 and future products available in Collection 6.1 (M*D = MYD/MOD for Aqua/Terra).

Product	Collection 6 (C6)	Collection 6.1 (C6.1)
L2 swath	M*D21 (LST, emissivity bands 29,31,32) M*D11 (LST, emissivity bands 31,32)	M*D21 (LST, emissivity bands 29,31,32) M*D11 (LST, emissivity bands 31,32)
L3 Daily Gridded	M*D21A1 (LST, emissivity bands 29,31,32) M*D11A1 (LST, emissivity bands 31,32) M*D11B1 (Day-Night product) (LST, 6 emissivity bands 20,22,23,29,31,32)	M*D21A1 (LST, emissivity bands 29,31,32) M*D11A1 (LST, emissivity bands 31,32) M*D11B1 (Day-Night product) (LST, 6 emissivity bands 20,22,23,29,31,32)
L3 8-day Gridded	M*D21A2 (LST, emissivity bands 29,31,32) M*D11A2 (LST, emissivity bands 31,32)	M*D21A2 (LST, emissivity bands 29,31,32) M*D11A2 (LST, emissivity bands 31,32)
L3 Climate Modeling Grids	M*D11C1 (daily, LST, 6 emissivity bands) M*D11C2 (8-day, LST, 6 emissivity bands) M*D11C3 (monthly, LST, 6 emissivity bands)	M*D21C1 (daily, LST, 3 emissivity bands) M*D21C2 (8-day, LST, 3 emissivity bands) M*D21C3 (monthly, LST, 3 emissivity bands) M*D11C1 (daily, LST, 6 emissivity bands) M*D11C2 (8-day, LST, 6 emissivity bands) M*D11C3 (monthly, LST, 6 emissivity bands)

References

[1] Zhengming Wan and J. Dozier, "A generalized split-window algorithm for retrieving land-surface temperature from space," in *IEEE Transactions on Geoscience and Remote Sensing,* vol. 34, no. 4, pp. 892-905, July 1996, doi: 10.1109/36.508406.

[2] Zhengming Wan and Zhao-Liang Li, "A physics-based algorithm for retrieving land-surface emissivity and temperature from EOS/MODIS data," in *IEEE Transactions on Geoscience and Remote Sensing*, vol. 35, no. 4, pp. 980-996, July 1997, doi: 10.1109/36.602541.

[3] N. Malakar and G. C. Hulley, "A water vapor scaling model for improved land surface temperature and emissivity separation of MODIS thermal infrared data," *Remote Sens Environ,* vol. 182, pp. 252-264, 2016, doi: 10.1016/j.rse.2016.04.023.

[4] T. Islam, G. C. Hulley, N. K. Malakar, R. G. Radocinski, P. C. Guillevic and S. J. Hook, "A Physics-Based Algorithm for the Simultaneous Retrieval of Land Surface Temperature and Emissivity From VIIRS Thermal Infrared Data," *IEEE Transactions on Geoscience and Remote Sensing*, vol. 55, no. 1, pp. 563-576, Jan. 2017, doi: 10.1109/TGRS.2016.2611566.

[5] G. C. Hulley, N. K. Malakar, T. Islam and R. J. Freepartner, "NASA's MODIS and VIIRS Land Surface Temperature and Emissivity Products: A Long-Term and Consistent Earth System Data Record," in *IEEE Journal of Selected Topics in Applied Earth Observations and Remote Sensing*, vol. 11, no. 2, pp. 522-535, Feb. 2018, doi: 10.1109/JSTARS.2017.2779330.

[6] W. C. Snyder, Z. Wan, Y. Zhang & Y.-Z. Feng (1998) Classification-based emissivity for land surface temperature measurement from space, *International Journal of Remote Sensing,* 19:14, 2753-2774, DOI: 10.1080/014311698214497.

[7] Coll, C., Wan, Z., and Galve, J. M., "Temperature-based and radiance-based validations of the V5 MODIS land surface temperature product," *J. Geophys. Res.*, 114, D20102, 2009, doi:10.1029/2009JD012038.

[8] H. Li et al., "Temperature-Based and Radiance-Based Validation of the Collection 6 MYD11 and MYD21 Land Surface Temperature Products Over Barren Surfaces in Northwestern China," in *IEEE Transactions on Geoscience and Remote Sensing*, doi: 10.1109/TGRS.2020.2998945.

[9] G. C. Hulley and S. J. Hook, "Intercomparison of Versions 4, 4.1 and 5 of the MODIS Land Surface Temperature and Emissivity Products and Validation with Laboratory Measurements of Sand Samples from the Namib Desert, Namibia," *Remote Sens Environ,* vol. 113, pp. 1313-1318, 2009.

[10] A. N. French, T. J. Schmugge, J. C. Ritchie, A. Hsu, F. Jacob, and K. Ogawa, "Detecting land cover change at the Jornada Experimental Range, New Mexico with ASTER emissivities," *Remote Sens Environ,* vol. 112, no. 4, pp. 1730-1748, Apr 15 2008, doi: 10.1016/j.rse.2007.08.020.

[11] S. W. Seemann, E. E. Borbas, R. O. Knuteson, G. R. Stephenson, and H. L. Huang, "Development of a global infrared land surface emissivity database for application to clear sky sounding retrievals from multispectral satellite radiance measurements," *J Appl Meteorol Clim,* vol. 47, no. 1, pp. 108-123, Jan 2008, doi: 10.1175/2007jamc1590.1.

[12] E. E. Borbas, G. Hulley, M. Feltz, R. Knuteson, and S. Hook, "The Combined ASTER MODIS Emissivity over Land (CAMEL) Part 1: Methodology and High Spectral Resolution Application," (in English), *Remote Sens-Basel,* vol. 10, no. 4, Apr 2018, doi: A10.3390/Rs10040643.

[13] A. Gambacorta et al., "An Experiment Using High Spectral Resolution CrIS Measurements for Atmospheric Trace Gases: Carbon Monoxide Retrieval Impact Study," in *IEEE Geoscience and Remote Sensing Letters*, vol. 11, no. 9, pp. 1639-1643, Sept. 2014, doi: 10.1109/LGRS.2014.2303641.

[14] Z. G. Yao, J. Li, J. L. Li, and H. Zhang, "Surface Emissivity Impact on Temperature and Moisture Soundings from Hyperspectral Infrared Radiance Measurements," *J Appl Meteorol Clim,* vol. 50, no. 6, pp. 1225-1235, Jun 2011, doi: 10.1175/2010jamc2587.1.

[15] G. C. Hulley, S. J. Hook, and A. M. Baldridge, "Investigating the Effects of Soil Moisture on Thermal Infrared Land Surface Temperature and Emissivity Using Satellite Retrievals and Laboratory Measurements," *Remote Sens Environ,* vol. 114, pp. 1480-1493, 2010.

[16] M. Mira, E. Valor, R. Boluda, V. Caselles, and C. Coll, "Influence of soil water content on the thermal infrared emissivity of bare soils: Implication for land surface temperature determination," *Journal of Geophysical Research-Earth Surface,* vol. 112, no. F4, p. F04003, Oct 23 2007, doi: 10.1029/2007jf000749.

[17] H. Tonooka and K. Kondo, "Comparison of surface emissivity ratio and surface wind environment in Dry Valley, Antarctica," in *28th Asian conference on remote sensing (ACRS 2007)*, Kuala Lumpur, Malaysia, Nov. 2007 2007, vol. PS2.G3.6.

[18] G. Hulley, S. Veraverbeke, and S. Hook, "Thermal-based techniques for land cover change detection using a new dynamic MODIS multispectral emissivity product (MOD21)," *Remote Sens Environ,* vol. 140, pp. 755-765, Jan 2014, doi: 10.1016/j.rse.2013.10.014.

[19] C. Coll, V. García-Santos, R. Niclòs and V. Caselles, "Test of the MODIS Land Surface Temperature and Emissivity Separation Algorithm With Ground Measurements Over a Rice Paddy," in *IEEE Transactions on Geoscience and Remote Sensing*, vol. 54, no. 5, pp. 3061-3069, May 2016, doi: 10.1109/TGRS.2015.2510426.

[20] S. L. Ermida, I. F. Trigo, C. C. DaCamara, F. M. Gottsche, F. S. Olesen, and G. Hulley, "Validation of remotely sensed surface temperature over an oak woodland landscape - The problem of viewing and illumination geometries," *Remote Sens Environ,* vol. 148, pp. 16-27, May 25 2014, doi: 10.1016/j.rse.2014.03.016.

[21] G. Hulley, S. Hook, and C. Hughes, "MODIS MOD21 Land Surface Temperature and Emissivity Algorithm Theoretical Basis Document," Jet Propulsion Laboratory, California Institute of Technology, *JPL Publication 12-17*, August, 2012.